analytical chemistry

pubs.acs.org/ac Letter

Construction of an Integrated Device of a Self-Powered Biosensor and Matching Capacitor Based on Graphdiyne and Multiple Signal Amplification: Ultrasensitive Method for MicroRNA Detection

Yang-Yang Hou, Jing Xu, Fu-Ting Wang, Zhong Dong, Xuecai Tan, Ke-Jing Huang,* Jia-Qiang Li,* Chun-Yang Zuo, and Si-Qi Zhang

Cite This: *Anal. Chem.* 2021, 93, 15225−15230 Read Online

ACCESS | Metrics & More | Article Recommendations | Supporting Information

ABSTRACT: The detection of microRNA (miRNA) in human serum has great significance for cancer prevention. Herein, a novel self-powered biosensing platform is developed, which effectively integrates an enzymatic biofuel cell (EBFC)-based self-powered biosensor with a matching capacitor for miRNA detection. A catalytic hairpin assembly and hybrid chain reaction are used to improve the analytical performance of EBFC. Furthermore, the matching capacitor is selected as an auxiliary signal amplifying device, and graphdiyne is applied as substrate material for EBFC. The results confirm that the developed method obviously increases the output current of EBFC, and the sensitivity can reach 2.75 μA/pM, which is 786% of pure EBFC. MiRNA can be detected in an expanded linear range of 0.1−100000 fM with a detection limit of 0.034 fM (S/N = 3). It can offer a selective and sensitive platform for nucleotide sequence detection with great potential in clinical diagnostics.

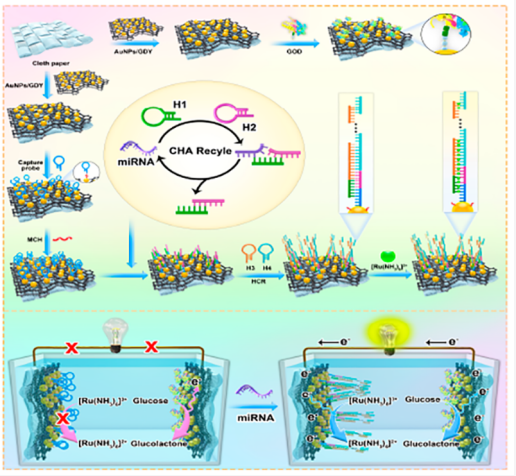

Enzymatic biofuel cells (EBFCs) can produce electrical energy from biomass fuel by enzymatic reactions.[1,2] In comparison with conventional electrochemical sensors, self-powered sensors based on EBFC are beneficial for reducing cost, have a simple structure, do not need a power supply, and have been widely used in the fields of chemistry, medicine, and environment.[3−6] As is known, substrate sources directly determine the electrochemical performances of EBFCs. Thus, the substrate sources of big superficial areas, good biocompatibilities, and conductive abilities are attractive.

Carbon ingredients have been widely applied in building EBFCs recently due to their excellent physicochemical property.[7,8] Being a brand-new type of carbon material, graphdiyne (GDY) has attracted wide attention due to its unique advantages of excellent electrochemical properties, good chemical stability, and large specific surface area.[9,10] Currently, GDY has been applied in energy storage,[11] solar cells,[12] catalysis,[13] and sensors.[14] However, there is no report about using GDY as the electrode material for EBEC construction.

Oligonucleotide-based signal amplification is a useful method to improve detection sensitivity, manly including nuclease signal amplification and enzyme-free assembled DNA signal amplification.[15−17] Therefore, it would be a good choice to combine GDY and oligonucleotide-based signal amplification to significantly improve the performance of EBFCs.

Introducing a highly efficient energy storage device to self-powered electrochemical biosensors is another direct and effective method to improve sensitivity. The capacitor has high power density and can realize instantaneous rapid charge and discharge. Zhang et al.[18] introduced a capacitor into a self-powered photoelectrochemical aptasensor, which was 8.7 times better than a pure self-powered PEC aptasensor on sensitivity. Yu et al.[19] designed a sensing platform by integrating a supercapacitor with a biological fuel cell with 13-fold higher sensitivity than that without a supercapacitor.

Herein, an ultrasensitive self-powered biosensing platform is assembled based on an EBFC and a capacitor for miRNA detection. The detailed diagram of the fabrication of the self-powered biosensor is shown in Scheme 1. AuNPs/GDY is dropped on a CP electrode as the substrate of the bioanode and biocathode. After glucose oxidase (GOD) is immobilized on AuNPs/GDY-modified CP, the bioanode is obtained. Parallelly,

Received: August 17, 2021
Accepted: November 2, 2021
Published: November 9, 2021

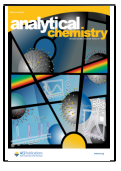

Downloaded via 208.99.107.11 on November 3, 2022 at 19:02:17 (UTC).
See https://pubs.acs.org/sharingguidelines for options on how to legitimately share published articles.

ACS Publications © 2021 American Chemical Society

https://doi.org/10.1021/acs.analchem.1c03521
Anal. Chem. 2021, 93, 15225−15230

Scheme 1. Detailed Diagram of Fabrication of Self-Powered Biosensor

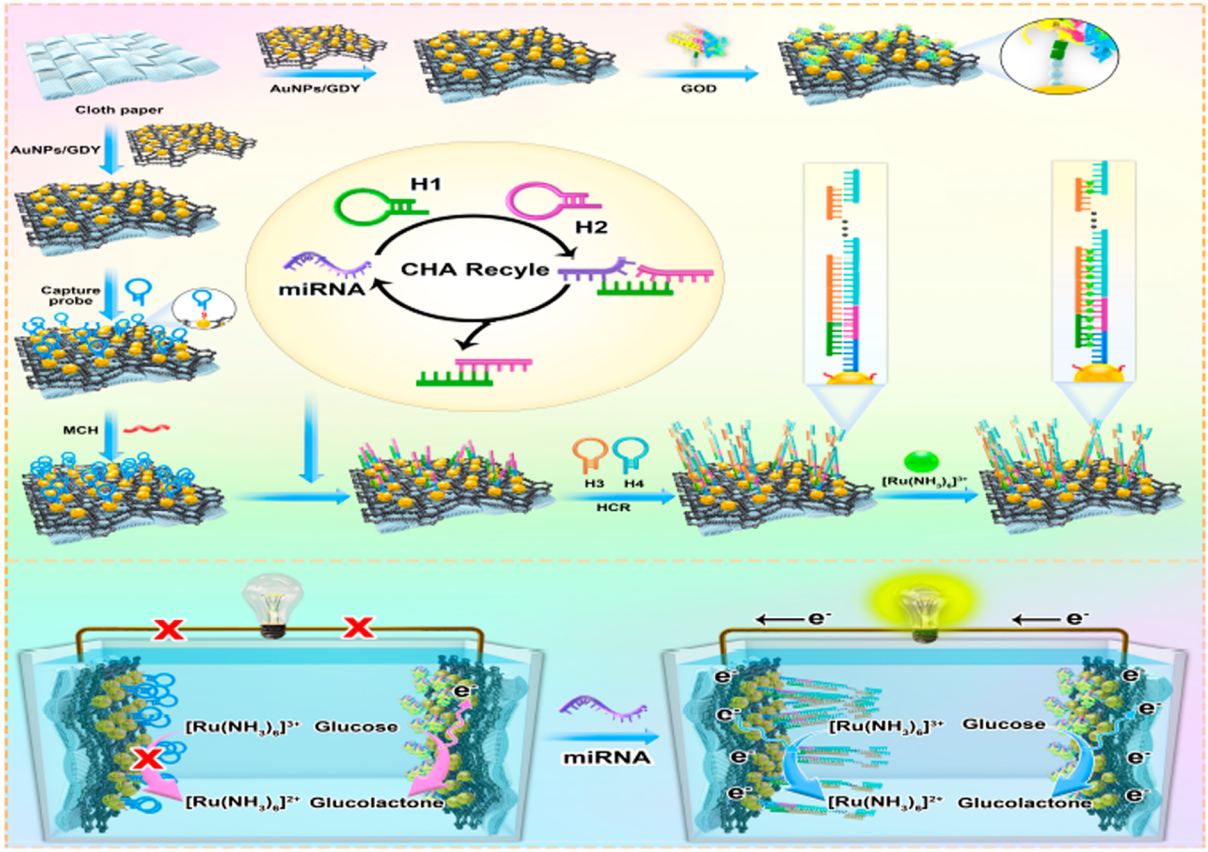

Scheme 2. Detailed Diagram Capacitor/EBFC Hybrid Device

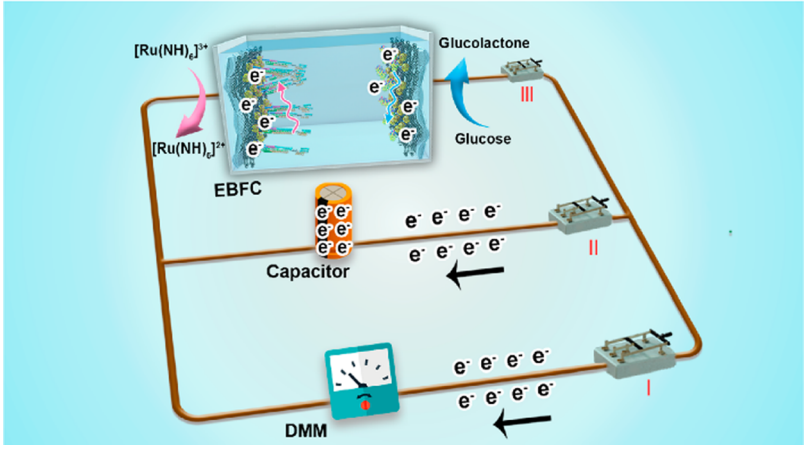

for biocathode fabrication, a capture probe is first fixed on the AuNPs/GDY-modified CP by the Au−S bond to get SH-CP. In the absence of miRNA, the hairpin structure of SH-CP remains closed, and subsequent reactions cannot initiate, resulting in a low E^{OCV}. When miRNA exists, CHA is triggered, and the hairpin structures of H1 and H2 are opened successively. MiRNA first binds to H1. Subsequently, H2 displaces miRNA and binds to H1, and the CHA target miRNA recycling promotes rapid generation of the CHA product H1−H2. Thus, CHA products are immobilized on the electrode surface by specifically binding to SH-CP. Then, the hairpin structures of H3 and H4 are successively opened to trigger a HCR reaction, and a long double-helix DNA chain is produced. Then, an electron acceptor $[Ru(NH_3)_6]^{3+}$ is inserted into a double-helix chain by an electrostatic interaction. Subsequently, electrons from glucose oxidation are transmitted to the biocathode; thus, $[Ru(NH_3)_6]^{3+}$ can decline to $[Ru(NH_3)_6]^{2+}$, which produces a high E^{OCV}.

Furthermore, a matching capacitor is introduced into EBFC construction for further improving the performance of the biosensor. The detailed diagram of the fabrication of the capacitor/EBFC hybrid device is shown in Scheme 2. The hybrid device mainly includes an EBFC, a capacitor, and a digital multimeter (DMM). Its working process is shown in SI. In this design, an EBFC is used as a power source to charge the capacitor through voltage. Subsequently, the capacitor releases a

https://doi.org/10.1021/acs.analchem.1c03521
Anal. Chem. 2021, 93, 15225−15230

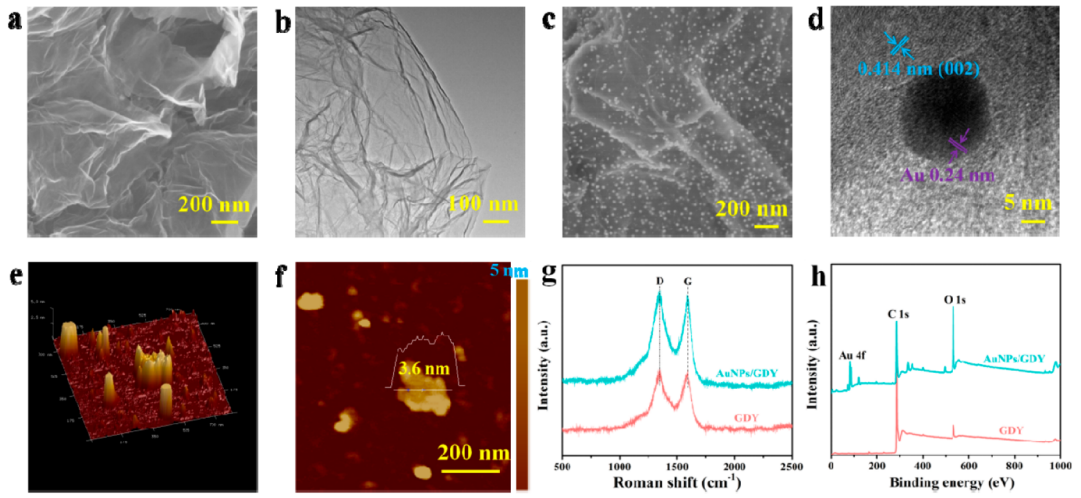

Figure 1. SEM (a) and TEM (b) of GDY nanosheets. SEM (c) and HRTEM (d) images of AuNPs/GDY cosmposite. (e–f) AFM images of GDY nanosheets. Raman (g) and XPS survey spectra (h) of GDY and AuNPs/GDY.

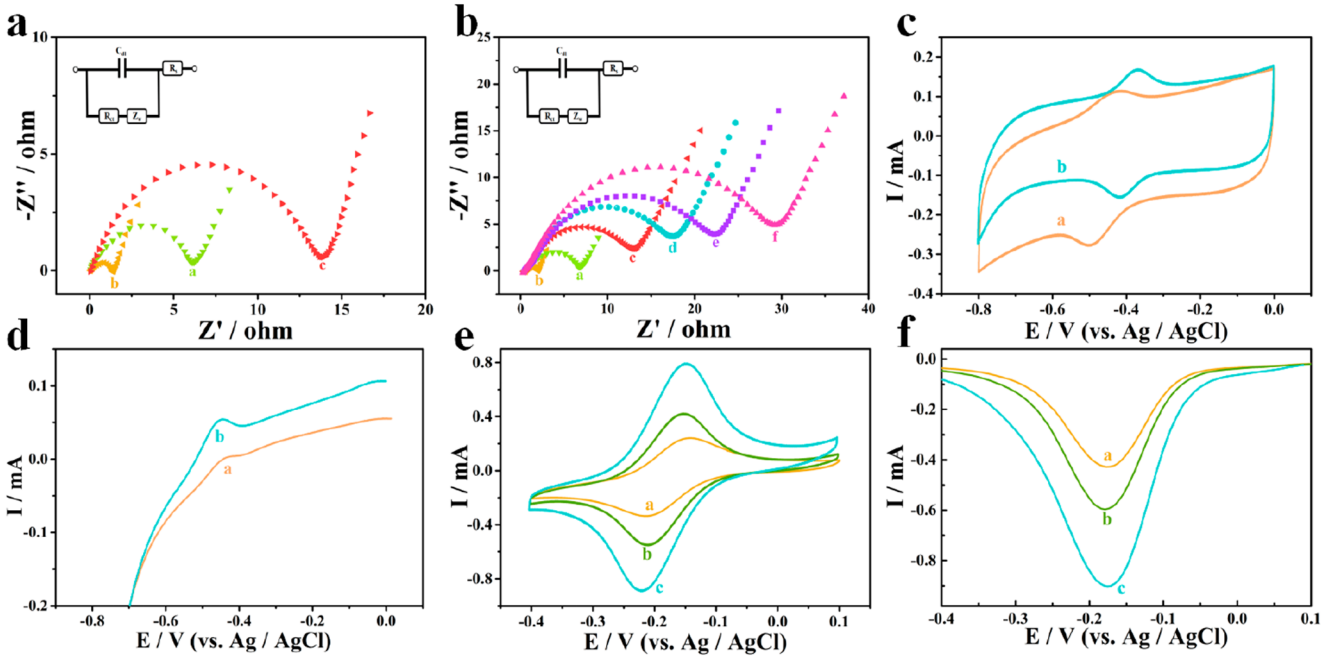

Figure 2. (a) EIS of bioanode: (a) CP, (b) AuNPs/GDY/CP, (c) GOD/AuNPs/GDY/CP. (b) EIS of biocathode: (a) CP, (b) AuNPs/GDY/CP, (c) SH-CP/AuNPs/GDY/CP. (d) MCH/SH-CP/AuNPs/GDY/CP. (e) H2/H1/miRNA-21/MCH/SH-CP/AuNPs/GDY/CP. (f) H4/H3/H2/H1/miRNA-21/MCH/SH-CP/AuNPs/GDY/CP. CVs (c) and LSVs (d) of the bioanode in PBS (pH 7.4) without glucose (curve a) and with 5 mM glucose (curve b). CVs (e) and LSVs (f) of biocathode to DNA hybrid level. (a–c) SH-CP/MCH, SH-CP + miRNA-21 + H1 + H2, SH-CP + miRNA-21 + H1+ H2 + H3 + H4. The concentrations of capture probe, H1/H2, and H3/H4 were 1 μM, and the level of miRNA-21 was 1 pM.

greatly amplified instantaneous current and is detected by DMM, which is several times bigger than the EBFC without the capacitor. The proposed hybrid device effectively combines the characteristics of self-powered biosensors, GDY, an oligonucleotide-based signal amplification and capacitor, showing excellent performance for miRNA detection.

RESULTS AND DISCUSSION

As shown in Figure 1a and b, GDY nanosheets show ultrathin layered structures. Figure 1c displays numerous AuNPs uniformly anchored on the surfaces of GDY nanosheets. The lattice margins of GDY and AuNPs are shown in Figure 1d. The streak spacing is about 0.24 and 0.414 nm, corresponding to Au (111) and GDY (002) crystal planes, respectively. AFM was used to further reveal structure information on the GDY. Figure 1e shows the ultrathin layered structure of GDY nanosheets. As shown in Figure 1f, the thicknesses of the GDY nanosheets are only 3.6 nm, which is beneficial to shorten the ion diffusion path. The Raman spectra of GDY and AuNPs/GDY are shown in Figure 1g. The *D* vertex point at 1348.6 cm^{-1} is due to presence of edge and amorphous carbons. The *G* peak at 1588 cm^{-1} indicates vibrations of C–C connections between triply coordinated atoms and their double-coordinated neighbors. The Raman signals of AuNPs/GDY significantly increase when compared with GDY. A possible reason is that the AuNPs can enhance the Raman signal of the AuNPs/GDY composite.[20]

https://doi.org/10.1021/acs.analchem.1c03521
Anal. Chem. 2021, 93, 15225–15230

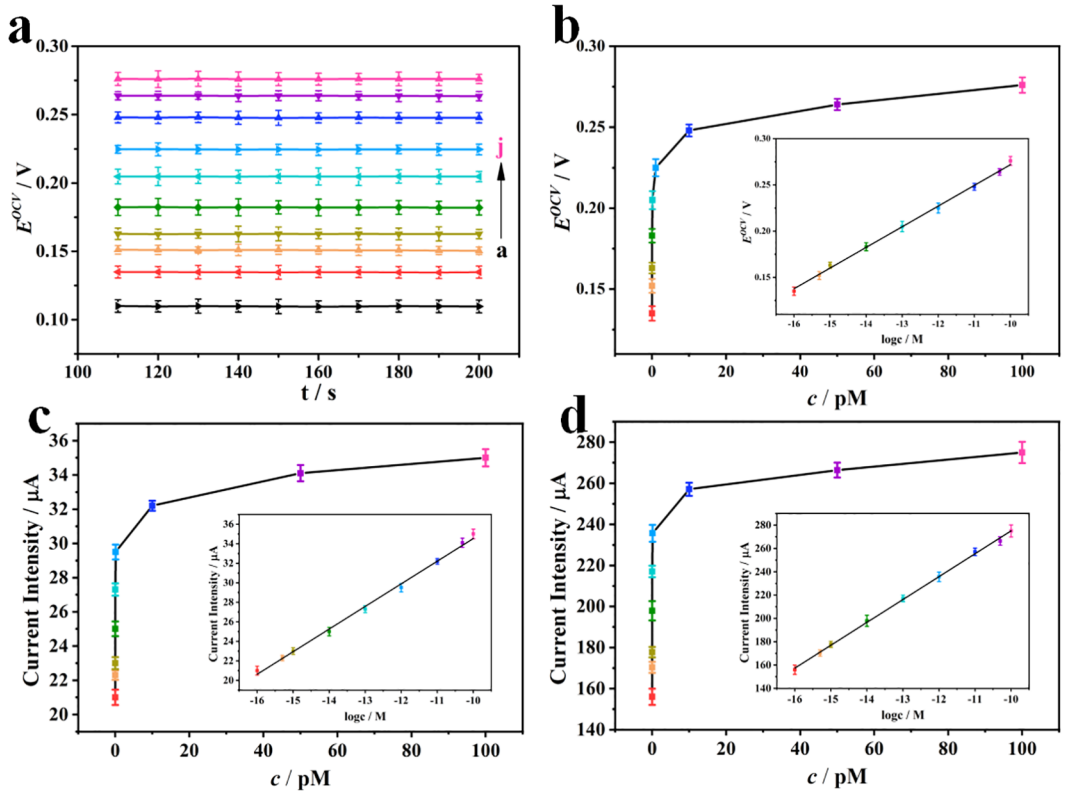

Figure 3. (a) E^{OCV} of self-powered biosensor of different miRNA-21 (a−j: 0, 0.1, 0.5, 1, 10, 100, 1000, 10000, 50000, 100000 fM). (b) Relation variation of E^{OCV} and miRNA-21 levels, and inset is the linear relationship between E^{OCV} and miRNA concentrations. The variation of instantaneous current as a function of miRNA concentration without capacitor (c) or with capacitor (d); the inset is the linear relationship between the instantaneous current and concentrations of miRNA.

The characteristic peaks of C 1s, O 1s, and Au 4f are observed in Figure 1h, further confirming the successful immobilization of AuNPs on GDY. Furthermore, XPS spectra and BET results of GDY are shown in the Supporting Information. The electrochemical properties of the GDY nanomaterial was also investigated and is displayed in the Supporting Information. The results confirm that GDY can greatly enhance the enzyme loading quantity and promote electron transfer.

The stepwise assembly process of a biosensor was verified by EIS. As shown in Figure 2a, the R_{et} value of bare CP is about 5.8 Ω (curve a) . When AuNPs/GDY is modified on the CP, the R_{et} value obviously declines (curve b), due to the excellent conductivity of AuNPs/GDY. However, the R_{et} value remarkably increases (curve c) after being incubated with GOD, owing to the big spatial steric resistance of biomolecules. As shown in Figure 2b, the R_{et} value (curve c) further increases after incubation with a capture probe, which is due to the negative DNA skeleton rejecting $[Fe(CN)_6]^{3-/4-}$. After the reaction with MCH, the R_{et} value (curve d) continues to increase. When miRNA-21 and a mixed solution of H1/H2 are applied on the electrode, the R_{et} value keeps increasing (curve e), which indicates a successful CHA process. After being incubated with H3 and H4, the R_{et} value of the electrode reaches the maximum (curve f), indicating that the HCR process is triggered. The inset of the figure is the equivalent circuit for the fitting data.

The CV and LSV of a bioanode were recorded. As displayed in Figure 2c and d, in the absence of glucose, two obvious redox peaks of the bioanode appear at around −0.5 V (curve a), which are the characteristic peaks of GOD. Clearly, the oxidation peaks of CV and LSV increase when glucose is added to the substrate solution (curve b) because the oxidation of glucose needs consumption of O_2, and the deviation of the CV peak is possibly related to products of glucose oxidation.[21−23]

As shown in Figure 2e and f, CV and DPV are applied to explore the signal response of the biocathode. The peak current is weak when only the capture probe exists (curve a). When the biocathode reacts with miRNA-21 and further hybrids with H1 and H2, the peak current obviously increases (curve b) because CHA products appear on the electrode. Once H3 hybridizes with H4 on the biocathode, the HCR reaction is triggered to generate a long dsDNA chain, which attracts a large amount of $[Ru(NH_3)_6]^{3+}$ on the biocathode; therefore, the peak current obviously increases (curve c). What is exciting is that the values of the peak currents of CHA and HCR (curve c) is twice that of the pure CHA (curve b), which confirms that the dual signal amplification strategy can effectively improve the signal response of the sensor.

Various concentrations of miRNA were detected with the developed self-powered biosensor. In Figure 3a, the E^{OCV} value of the EBFC biosensor is very low without miRNA-21. However, the E^{OCV} value increases significantly once miRNA-21 is added. As is shown in Figure 3b, the E^{OCV} value linearly enhances with the increase of target miRNA concentrations. The linear range is 0.1−100000 fM, and the linear regression equation is E^{OCV} = 0.0224 log c + 0.49575 (correlation coefficient R^2 = 0.9970). The detection limit is 0.034 fM (S/N = 3), which is lower than other methods (Table S2). Moreover, different concentrates of miRNA were detected by the capacitor/EBFC hybrid device under the optimized condition. In Figure 3c, the instantaneous current increases with the rising of miRNA-21 concentration.

https://doi.org/10.1021/acs.analchem.1c03521
Anal. Chem. 2021, 93, 15225−15230

The inset of Figure 3c exhibits a linear relationship between the instantaneous available and logarithm of miRNA-21 levels in the range of 0.1−100000 fM. As shown in Figure 3d, the instantaneous current enhances obviously and remains in a good linear relationship after the capacitor amplification. The sensitivity (2.75 μA/pM) of the capacitor/EBFC hybrid device is improved by 786% compared to that without a capacitor. The results indicate that the capacitor can greatly improve the performance of the biosensor.

To assess the selectivity of the biosensor, three miRNAs (miR-141, miR-155, and miR-199a) and three mismatched sequence-based miR-21 (smRNA, tmRNA, and NC) were selected as interfering factors (1 pM). As shown Figure S6a, the ΔE^{OCV} values of these interferes are very low compared with target miRNA, showing the excellent selectivity of a self-powered biosensor. The proposed self-powered biosensors were kept at 4 °C for 3, 6, 9, and 12 days to evaluate the long-term stability. As shown in Figure S6b, the E^{OCV} responses of the self-powered biosensor are maintained at 94.15%, 95.56%, and 93.56% of the original E^{OCV} to miRNA-21 at concentrations of 10^{-13}, 10^{-12}, and 10^{-11} mol mL^{-1} even after 12 days. The result demonstrates the excellent stability of the self-powered biosensor. Five independently manufactured self-powered biosensors were used to repeatedly detect miRNA of 10^{-13}, 10^{-12}, and 10^{-11} mol mL^{-1} to evaluate the reproducibility. As seen in Figure S6c, relative standard deviations (RSDs) of 2.3%, 2.49%, and 2.92% are obtained, respectively, confirming the outstanding reproducibility of the self-powered biosensor.

The applicability of the designed biosensor was evaluated. The human serum samples (obtained from attached hospital of Xinyang normal University) were measured. As shown in Table S3, the recoveries of 96.74%−106.7% and the RSDs of 3.33%−5.71% are obtained, confirming the validity of the method for detection of miRNA-21 in the real sample.

CONCLUSIONS

The application of GDY in EBFC-based self-powered biosensing platform construction is explored, and the platform presents two novel definitions. First, GDY used as electrode substrate shows high enzyme load quantity and excellent conductivity, which can greatly improve the analysis performance of a self-powered biosensor. Second, the introduction of oligonucleotide-based signal amplification and capacitors to the self-powered biosensor fabrication can significantly improve its sensitivity. The resulted hybrid device shows a wide linear range and a low detection limit. In particular, the introduction of capacitors has significantly increased the sensitivity of the sensor to 786% of that without a capacitor. Its desirable properties determine that this method has great potential applications in clinical treatment.

ASSOCIATED CONTENT

Supporting Information

The Supporting Information is available free of charge at https://pubs.acs.org/doi/10.1021/acs.analchem.1c03521.

Experimental section, XPS spectra, and BET for prepared samples; optimization of experimental conditions; electrochemical properties of of GDY; results of specificity, stability; and reproducibility of the assay; table of sequences of oligonucleotides; table of results of different sensors for miRNA detection; and table of results of miRNA−21 in human serum samples (PDF)

AUTHOR INFORMATION

Corresponding Authors

Ke-Jing Huang − *College of Chemistry and Chemical Engineering, Xinyang Normal University, Xinyang 464000, China; Key Laboratory of Chemistry and Engineering of Forest Products, Guangxi Key Laboratory of Chemistry and Engineering of Forest Products, Key Laboratory of Guangxi Colleges and Universities for Food Safety and Pharmaceutical Analytical Chemistry, School of Chemistry and Chemical and Engineering, Guangxi University for Nationalities, Nanning 530008, China*; Email: kejinghuang@163.com

Jia-Qiang Li − *Advanced Membranes and Porous Materials Center, Physical Sciences and Engineering Division, King Abdullah University of Science and Technology, Thuwal 23955-6900, Saudi Arabia*; Email: jiaqiang.li@kaust.edu.sa

Authors

Yang-Yang Hou − *College of Chemistry and Chemical Engineering, Xinyang Normal University, Xinyang 464000, China*; orcid.org/0000-0002-7233-6385

Jing Xu − *College of Chemistry and Chemical Engineering, Xinyang Normal University, Xinyang 464000, China*

Fu-Ting Wang − *College of Chemistry and Chemical Engineering, Xinyang Normal University, Xinyang 464000, China*

Zhong Dong − *College of Chemistry and Chemical Engineering, Xinyang Normal University, Xinyang 464000, China*

Xuecai Tan − *Key Laboratory of Chemistry and Engineering of Forest Products, Guangxi Key Laboratory of Chemistry and Engineering of Forest Products, Key Laboratory of Guangxi Colleges and Universities for Food Safety and Pharmaceutical Analytical Chemistry, School of Chemistry and Chemical and Engineering, Guangxi University for Nationalities, Nanning 530008, China*

Chun-Yang Zuo − *College of Chemistry and Chemical Engineering, Xinyang Normal University, Xinyang 464000, China*

Si-Qi Zhang − *College of Chemistry and Chemical Engineering, Xinyang Normal University, Xinyang 464000, China*

Complete contact information is available at: https://pubs.acs.org/10.1021/acs.analchem.1c03521

Notes

The authors declare no competing financial interest.

ACKNOWLEDGMENTS

The authors acknowledge financial support from the Natural Science Foundation of China (22074130, 21365004) and Zhongyuan Thousand Talents Plan-Science and Technology Innovation Leading Talents Project (204200510030). The authors acknowledge the support from the Analysis Testing Center of Xinyang Normal University for the materials characterization.

REFERENCES

(1) Pinyou, P.; Blay, V.; Muresan, L.; Noguer, T. *Mater. Horiz.* **2019**, *6*, 1336−1358.

(2) Chansaenpak, K.; Kamkaew, A.; Lisnund, S.; Prachai, P.; Ratwirunkit, P.; Jingpho, T.; Blay, V.; Pinyou, P. *Biosensors.* **2021**, *11*, 16.

(3) Cheng, J.; Han, Y.; Deng, L.; Guo, S. J. *Anal. Chem.* **2014**, *86*, 11782−11788.

(4) Li, X.; Li, D.; Zhang, Y.; Lv, P.; Feng, Q.; Wei, Q. *Nano Energy.* **2020**, *68*, 104308.
(5) Xiao, X. X.; McGourty, K. D.; Magner, E. *J. Am. Chem. Soc.* **2020**, *142* (26), 11602−11609.
(6) Kung, C. T.; Hou, C. Y.; Wang, Y. N.; Fu, L. M. *Sens. Actuators, B.* **2019**, *301*, 126855.
(7) Wang, F. T.; Wang, Y. H.; Xu, J.; Huang, K. J.; Liu, Z. H.; Lu, Y. F.; Wang, S. Y.; Han, Z. W. *Nano Energy.* **2020**, *68*, 104310.
(8) Gu, C.; Gai, P.; Kong, X.; Hou, T.; Li, F. *Anal. Chem.* **2020**, *92*, 5426−5430.
(9) Baughman, R. H.; Eckhardt, H.; Kertesz, M. *J. Chem. Phys.* **1987**, *87*, 6687−6699.
(10) Huang, C.; Li, Y.; Wang, N.; Xue, Y.; Zuo, Z.; Liu, H.; Li, Y. *Chem. Rev.* **2018**, *118*, 7744−7803.
(11) Wang, F.; Zuo, Z. C.; Li, L.; He, F.; Li, Y. L. *Nano Energy.* **2020**, *68*, 104307.
(12) Li, H.; Zhang, R.; Li, Y.; Li, Y.; Liu, H.; Shi, J.; Zhang, H.; Wu, H.; Luo, Y.; Li, D.; Li, Y.; Meng, Q. *Adv. Eng. Mater.* **2018**, *8*, 1802012.
(13) Du, Y. C.; Xue, Y. R.; Zhang, C.; Liu, Y. X.; Fang, Y.; Xing, C. Y.; He, F.; Li, Y. L. *Adv. Energy Mater.* **2021**, *11*, 2100234.
(14) Parvin, N.; Jin, Q.; Wei, Y.; Yu, R.; Zheng, B.; Huang, L.; Zhang, Y.; Wang, L.; Zhang, H.; Gao, M.; Zhao, H.; Hu, W.; Li, Y.; Wang, D. *Adv. Mater.* **2017**, *29*, 1606755.
(15) Peng, H.; Newbigging, A. M.; Reid, M. S.; Uppal, J. S.; Xu, J.; Zhang, H.; Le, X. C. *Anal. Chem.* **2020**, *92*, 292−308.
(16) Wei, X. W.; Bian, F. K.; Cai, X. X.; Wang, Y.; Cai, L. J.; Yang, J.; Zhu, Y. F.; Zhao, Y. J. *Anal. Chem.* **2020**, *92*, 6121−6127.
(17) Wang, R.; Zhao, X.; Chen, X.; Qiu, X.; Qing, G.; Zhang, H.; Zhang, L.; Hu, X.; He, Z.; Zhong, D.; Wang, Y.; Luo, Y. *Anal. Chem.* **2020**, *92*, 2176−2185.
(18) Chen, Y. X.; Ji, W. H.; Gao, J.; Yan, K.; Zhang, J. D. *Chem. Commun.* **2020**, *56*, 10034−10037.
(19) Wang, Y. H.; Ge, L.; Ma, C.; Kong, Q. K.; Yan, M.; Ge, S. G.; Yu, J. H. *Chem. - Eur. J.* **2014**, *20*, 12680.
(20) Li, Y. X.; Li, X. H.; Meng, Y. C.; Hun, X. *Biosens. Bioelectron.* **2019**, *130*, 269−275.
(21) Christwardana, M.; Kim, K.; Kwon, Y. *Sci. Rep.* **2016**, *6*, 30128.
(22) Kowalewska, B.; Jakubow, K. *Sens. Actuators, B.* **2017**, *238*, 852−861.
(23) Baghayeri, M.; Veisi, H.; Ghanei-Motlagh, M. *Sens. Actuators, B.* **2017**, *249*, 321−330.

https://doi.org/10.1021/acs.analchem.1c03521
Anal. Chem. 2021, 93, 15225−15230